MEASUREMENT AND CALCULATION OF LEVITATION FORCES BETWEEN MAGNETS AND GRANULAR SUPERCONDUCTORS

T.H. JOHANSEN, H. BRATSBERG, M. BAZILJEVICH, P.O. HETLAND and A.B. RIISE

Department of Physics, University of Oslo.
P.O. Box 1048, Blindern, 0316 Oslo 3, Norway.

Abstract – Recent developments indicate that exploitation of the phenomenon of magnetic levitation may become one of the most important near-term applications of high-T_c superconductivity. Because of this, the interaction between a strong permanent magnet(PM) and bulk high-T_c superconductor(HTSC) is currently a subject of much interest . We have studied central features of the mechanics of PM-HTSC systems of simple geometries. Here we report experimental results for the components of the levitation force, their associated stiffness and mechanical ac-loss. To analyse the observed behavior a theoretical framework based on critical-state considerations is developed. It will be shown that all the mechanical properties can be explained consistently at a quantitative level using a minimum of model parameters.

1. INTRODUCTION

A quantitative understanding of how the nonuniform fields of permanent magnets(PMs) magnetizes bulk high-T_c superconductors(HTSCs) stands central in developing levitation-type applications like frictionless bearing for rotors, torque couplers, vibration dampers etc.[1-3] It is also a key to understand how replicas of magnetic structures can be made using HTSCs.[4] One approach to these issues is to investigate various aspects of the magnetic force acting between PMs and HTSCs.

From magnetomechanics[5] a PM producing a field $\mathbf{B}_a$ will experience a force from a volume V of magnetization $\mathbf{M}$ equal to

$$\mathbf{F} = \int_V (\mathbf{M} \cdot \nabla)\, \mathbf{B}_a \, dV \ . \tag{1}$$

Thus the force results from two distinct factors; i) the magnitude of the magnetization which in the case of superconductors is determined by the distribution of persistent shielding currents, and ii) the degree of inhomogeneity in the applied field. Since the field produced by PMs of simple shapes can be readily computed, one should in principle be able to discuss all aspects of the levitation phenomenon once the magnetization behavior of the HTSC is at hand. However, in the literature one finds that analyses of this kind are most often carried out on a very general and qualitative basis. Although some model calculations have been reported[6-8] a physical picture that consistently describes at a quantitative level the various properties of the interaction is still lacking.

We have performed a series of measurements to reveal the detailed behavior of several central features of levitation forces. System configurations of sufficient simplicity were chosen in order to compare the observed behavior with analytical calculations. In this paper we describe the results of our investigation.

2. VERTICAL FORCE

The experimental set-up designed to measure the vertical force is shown in fig.1. The fully computerized apparatus uses a Mettler AE240 Delta Range electronic balance as force sensor. The

force versus distance measurements were done after the HTSC sample had been zero-field cooled to 77K in liquid nitrogen. Both the PM and HTSC were shaped as rectangular bars, and mounted in a configuration shown in detail below.

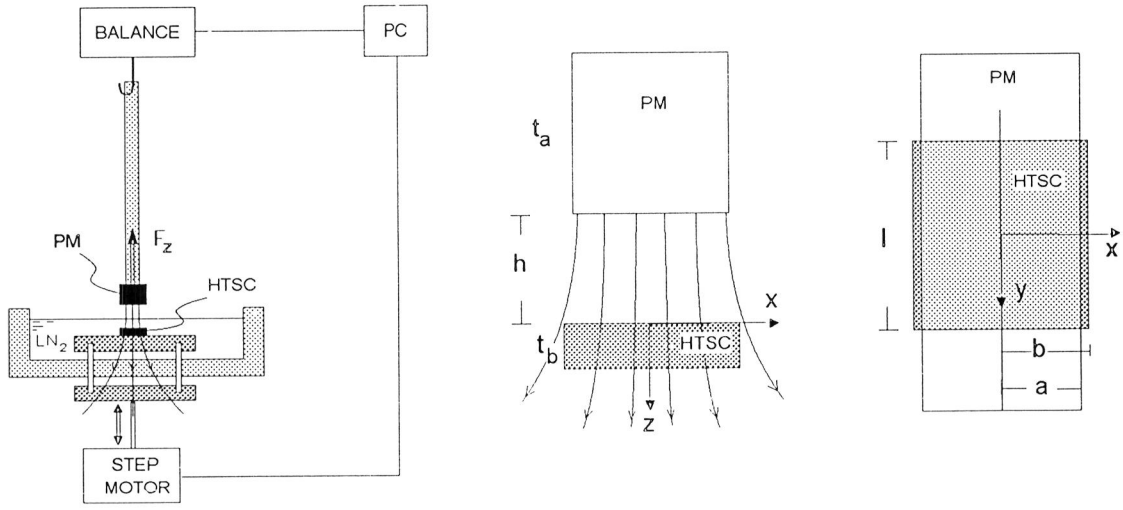

Figure 1: Apparatus to measure the vertical force between a PM and HTSC(left).
Magnet-superconductor configuration viewed along the y-axis(middle) and seen from above(right).

Using a step motor stage the force was measured while raising the HTSC towards the PM, starting from a distance $h = 20$ mm. At each point the collection of data was delayed in order to allow relaxations to decay below the 0.1mg resolution of the balance. At every millimeter the steady motion was interrupted for a reverse displacement of 15 μm. This added a set of minor loops in the F_z versus h curve. The result of the entire experiment is shown in fig.2(left).

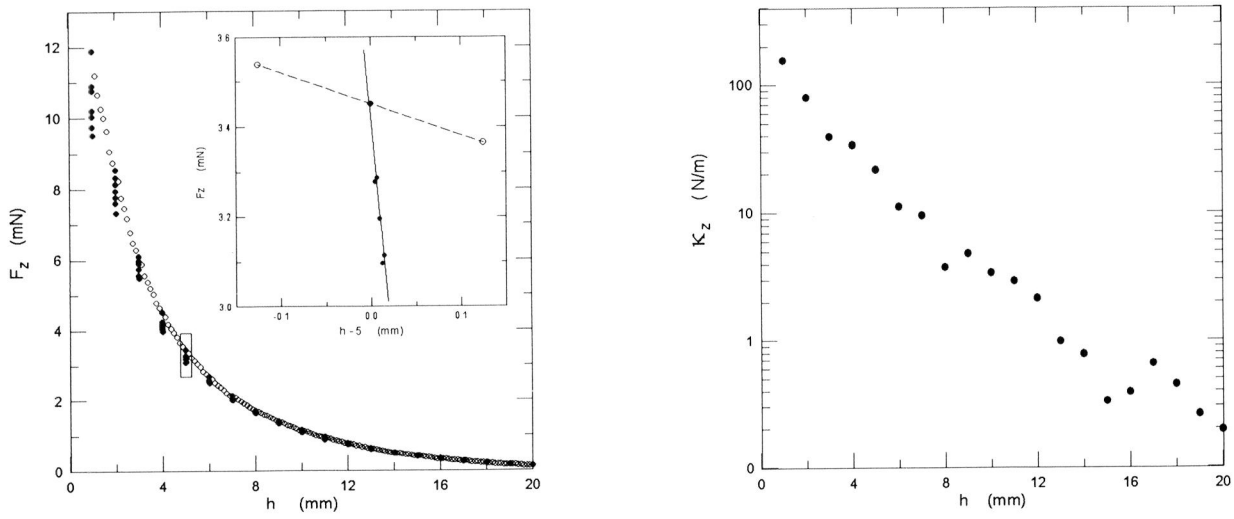

Figure 2: Vertical force as a function of PM-HTSC distance.(left) The insert shows a close-up of a minor loop. The magnetic stiffness versus levitation height is shown on the right.

The irreversible nature of the PM-HTSC interaction causes the minor loops to form an angle with the major curve. Thus, the spring constant, or stiffness, governing vibrational motion

needs to be determined separately. Note that hysteretic behavior can not be seen in the minor loops themselves, which make such small-amplitude oscillations essentially loss-free.[9] The vertical stiffness,

$$\kappa_z = -\frac{\delta F_z}{\delta h} ,$$

found as the slope of a line fitted to the individual minor loops is plotted in fig.2(right). The stiffness covers a range of 3 orders of magnitude, which makes it a parameter that varies much stronger than the force itself.

3. MODEL CALCULATION

The HTSC used in this study is made of $YBa_2Cu_3O_{7-\delta}$ prepared by a conventional sintering method. In order to construct a realistic model for our sample it is necessary to know, at least at a qualitative level, how an external field is penetrating the HTSC. In other words, what is the pattern of the induced shielding currents. An effective method to investigate this central point is to use a magneto-optic vizualization technique based on the Faraday effect in iron-garnet films with in-plane anisotropy.[10]. A plate serving as substrate for the thin indicator film is placed directly on the surface of the HTSC which is mounted in an optical cryostat. The contrast in the picture seen in a microscope with crossed polarizers gives an analoge representation of the perpendicular flux density at the HTSC surface.

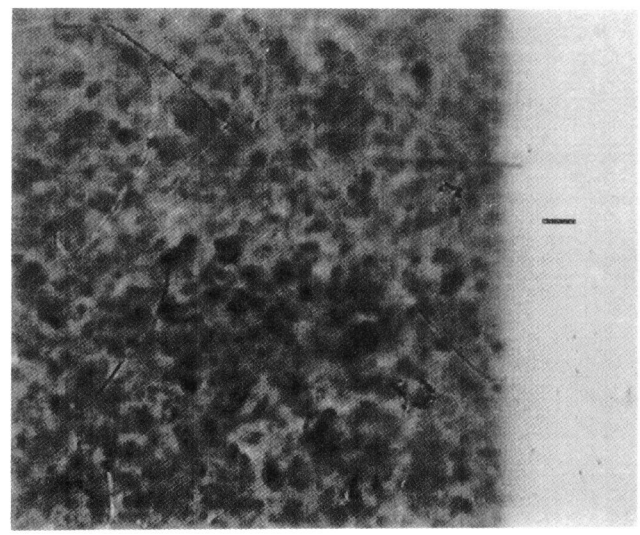

Figure 3: Magneto-optic image of flux penetration in our HTSC sample. The scale-bar is 100 μm long.

Figure 3 shows the image of our z.f.c. HTSC placed in an external field of 15mT at 15K. The edge of the sample is seen as the vertical line dividing the picture into two distinct regions. The uniform region to the right represents the intensity of the external field. In the left part one sees a complex structure of areas having nearly the same light intensity as outside the sample. The dark parts are regions of low flux intensity, i.e., where the superconductor is well shielded from the field. The HTSC can therefore be characterized as a magnetically porous material where the applied field leaks through the intergranular space, and thereby surrounding the grains which carry the shielding currents.

Evidently, it is formidable task in the calculation of levitation forces to account in detail for such complex magnetic structures as seen in the magneto-optic image. On the other hand, in the

present force experiments the size of the magnet is too large to feel the effect of individual grains, and one can therefore simplify the treatment by using a locally averaged magnetization. In the geometry of fig.1 this magnetization will be essentially vertical.

The dimensions of the HTSC sample are t_b = 1.7mm, b = 3.4mm and l = 11.9mm. The PM is made of Nd-Fe-B with a remanent induction of B_r=1.05T, and measures a = 2.8mm and t_a = 6.0mm. The length in the y–direction is 17mm, which is long compared to l, and hence the applied field is close to that of an infinitely long bar magnet, $\mathbf{B}_a = (B_x, 0, B_z)$, where

$$B_x(x,z) = \frac{B_r}{4\pi} \ln \frac{[(z+h)^2+(x+a)^2]\,[(z+h+t_a)^2+(x-a)^2]}{[(z+h)^2+(x-a)^2]\,[(z+h+t_a)^2+(x+a)^2]} \quad , \tag{2}$$

$$B_z(x,z) = \frac{B_r}{2\pi}\left(\arctan\frac{z+t_a+h}{a+x} + \arctan\frac{z+t_a+h}{a-x} - \arctan\frac{z+h}{a+x} - \arctan\frac{z+h}{a-x}\right) . \tag{3}$$

Making use of the approximation $\mathbf{M} = M(x,z)\,\hat{\mathbf{z}}$, the vertical force component equals

$$F_z = l \int_0^{t_b} dz \int_{-b}^{b} dx\; M\,\frac{\partial B_z}{\partial z} . \tag{4}$$

In order to make the calculations analytically tractable we will treat the HTSC as a system consisting of a large collection of decoupled grains, each behaving in accord with the critical state model.[11] The presence of pinning centres causes a gradient in the internal induction, which by Ampere's law is associated with an azimuthal current of density j_c. Figure 4 illustrates schematically the model behavior at various stages of the levitations force experiment.

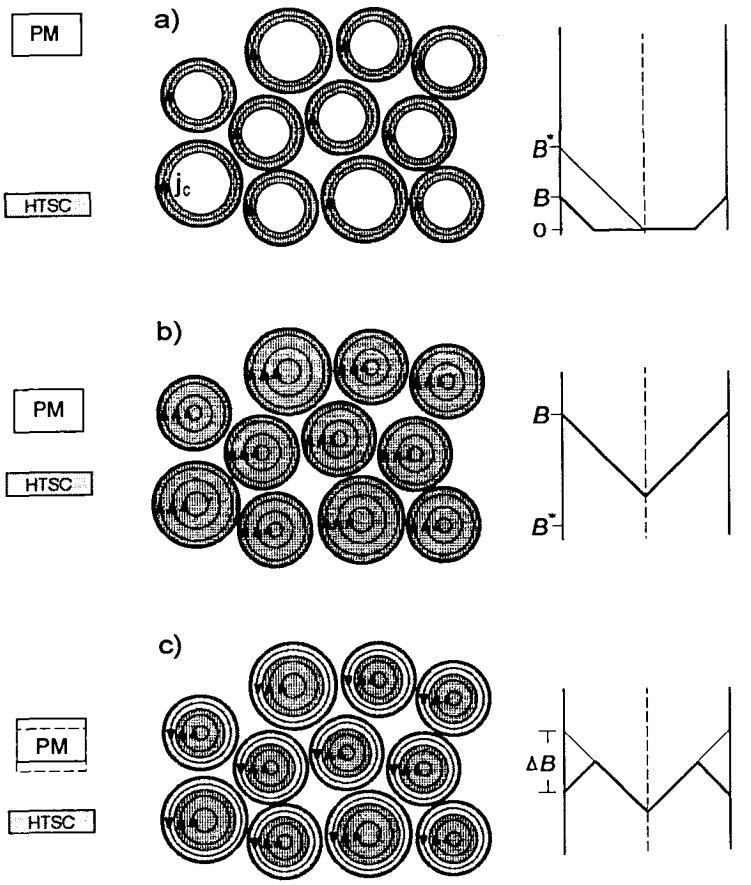

Figure 4: The decoupled grain model. a) Incomplete intra-granular flux penetration at a large PM-HTSC distance. b) At smaller distances the critical state is fully developed in the grains. c) After a small increase in PM-HTSC distance an outer layer of reversed j_c is formed.

Under conditions where essentially all grains are saturated with j_c, as in fig.4b, the magnetization can be considered uniform over the entire volume. In this case eq.(4) simplifies to

$$F_z = -M\, l \int_0^{t_b} 2\, B_x(b,z)\, dz\ . \tag{5}$$

Since the HTSC sample is relatively thin we make use of the approximation

$$F_z(h) = -2\, l\, t_b\, B_x(h)\, M\ , \tag{6}$$

where $B_x(h) \equiv B_x(b, t_b/2)$ in eq.(2).

Conditions of saturation can be expected to be realized at points on the enveloping part of the F_z versus h curve of fig.2 at the small-to-intermediate distances. Here the magnetization will be proportional to j_c. Since j_c is known to depend on the field it is instructive to make a parametric plot of $-M$, where

$$-M = \frac{F_z(h)}{2\, l\, t_b\, B_x(h)}\ , \tag{7}$$

against the applied field at corresponding values of h. This is done in fig.5, where the B-axis denotes the field at the centre of the sample, i.e., $B_z(h) \equiv B_z(0, t_b/2)$ in eq.(3).

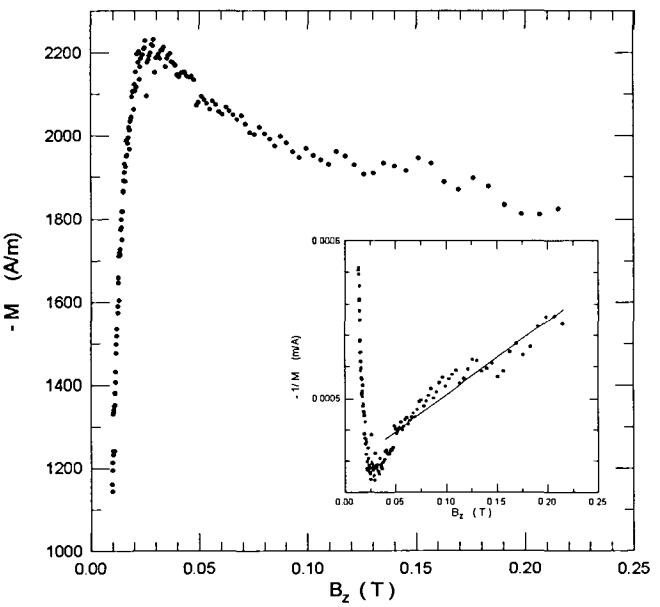

Figure 5: Parametric plot of the infered magnetization, eq.(7), against the applied field at the HTSC centre.

We see that $-M$ displays a clear peaked behavior, which can be understood as follows. As the HTSC approaches the PM the increasing applied field gradually magnetizes the grains. This gives rise to the steep positive flank of the curve. Saturation appears to occur near $B_z = 0.025$T, where $-M$ reaches its maximum. Above the maximum the field-dependence of j_c leads to a monotonic reduction in the magnetization. To quantify this behavior we use a form

$$-M = \frac{M_0}{1 + B_z/B_0}\ , \tag{8}$$

as in the Kim model.[12] The two parameters, M_0 and B_0, were determined by fitting a straight line to $1/M$ in the region indicated in the insert. This gave $M_0 = 2195$ A/m and $B_0 = 0.97$T.

By combining eq.(6) and (8) one can calculate the levitation force as function of the height h. The result is shown in fig.6 together with the enveloping part of the force data in fig.2. The

theoretical curve describes the behavior excellently from the smallest h and up to about 13mm. At larger distances a deviation starts appearing as a consequence of the non-saturation conditions, see fig.4a, existing at such small applied fields.

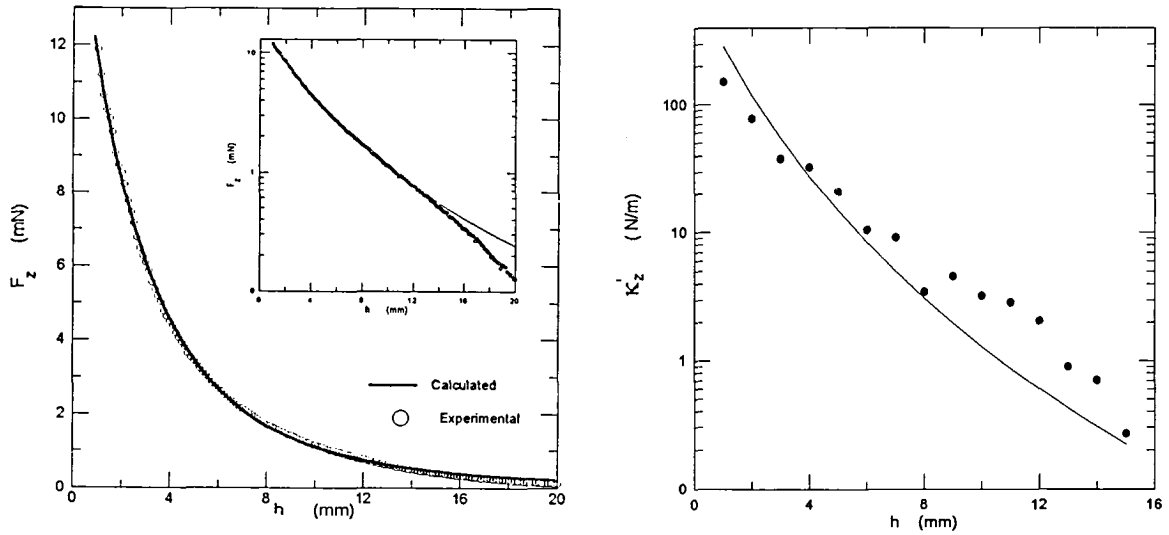

Figure 6: Measured levitation force together with fitted theoretical curve.(left) Semi-logarithmic plot of the vertical stiffness, κ', and the prediction of eq.(13).(right)

During the reversed vertical displacement producing the minor loops in fig.2, each grain will experience a reduction in the field. Some flux will pour out of the grain and establish in an outer layer a flux density gradient of opposite sign. As illustrated in fig.4c, this layer will now have j_c circulating in the reverse direction, giving a positive addition to the magnetization. If we for simplicity assumes that the grains have the shape of long cylinders the critical state model gives to first order

$$\mu_0 \Delta M_{grain} = |\frac{\partial B_z}{\partial z}| \, \Delta h \; . \tag{9}$$

After the PM-HTSC distance has been increased from h_0 to $h_0 + \Delta h$ the magnetization can then be written

$$M(h_0 + \Delta h) = M(h_0) + \frac{f_s}{\mu_0} \, |\frac{\partial B_z}{\partial z}| \, \Delta h \; , \tag{10}$$

where f_s is the volume fraction of the superconducting material. Again the force, $F_z(h_0 + \Delta h)$, can be found from eq.(4). If the state of magnetization at h_0 corresponds to saturation, i.e., $M(h_0) = -M_{sat}$, we get

$$F_z(h_0 + \Delta h) = l \int_0^{t_b} dz \int_{-b}^{b} dx \left(-M_{sat}(h_0) + \frac{f_s}{\mu_0} \, |\frac{\partial B_z}{\partial z}| \, \Delta h \right) \frac{\partial B_z}{\partial z} \; , \tag{11}$$

where the last gradient factor is evaluated for $h = h_0 + \Delta h$. Since the saturation magnetization varies slightly with $B_z(h)$ we write $M_{sat}(h_0)$ as $M_{sat}(h_0 + \Delta h) - (\partial M_{sat}/\partial h)_{h_0} \, \Delta h$. The first term here gives in eq.(11) the force at $h_0 + \Delta h$ on the enveloping curve. The two terms proportional to Δh quantifies how the stiffness deviates from the slope of the envelope. Using eq.(8) to represent M_{sat} one finds that the $\partial M_{sat}/\partial h$-term is negligibly small, leaving

$$\Delta F_z' = -\frac{f_s}{\mu_0} \, l \int_0^{t_b} dz \int_{-b}^{b} dx \left(\frac{\partial B_z}{\partial z} \right)^2 \Delta h \; , \tag{12}$$

to describe the angle of a minor loop. This irreversible reduction in the force gives the contribution to the stiffness

$$\kappa_z' = -\frac{\Delta F_z'}{\Delta h} = \frac{f_s}{\mu_0}\, 2\, l\, t_b \int_0^b \left(\frac{\partial B_z}{\partial z}\right)^2 dx \,. \tag{13}$$

Again, since our sample is thin we multiply here by t_b instead of integrating over z, and evaluate the gradient at $z = t_b/2$.

Using the data of fig.2(left) the experimental κ_z' was derived and compared with the theoretical result, eq.(13). Note that this comparison only allows for an adjustment of the prefactor,f_s, and is therefore a strong test of the physical model. Figure 6(right) shows the outcome of this procedure carried out for $h \leq 15$mm. The good quantitative agreement was obtained using $f_s = 0.8$, a most realistic value. The irreversible part κ_z' differs only very slightly from the full κ_z. Thus, from our analysis we conclude that the vertical stiffness is essentially independent of the actual magnetization of the HTSC. Geometrical parameters together with the gradient of the applied field are the most important.

4. HORIZONTAL INTERACTION

It is a well known feature of the PM-HTSC interaction that it can provide lateral stability, i.e., a horizontal restoring force will prevent e.g. a magnet to fall to one side when it is placed levitating above a superconductor. In a previous work we investigated[13] this stabilizing force together with the stiffness that governs lateral vibrational motion. We include these experimental results here to show that the theoretical framework developed in the previous section also describes the behavior of the horizontal interaction.

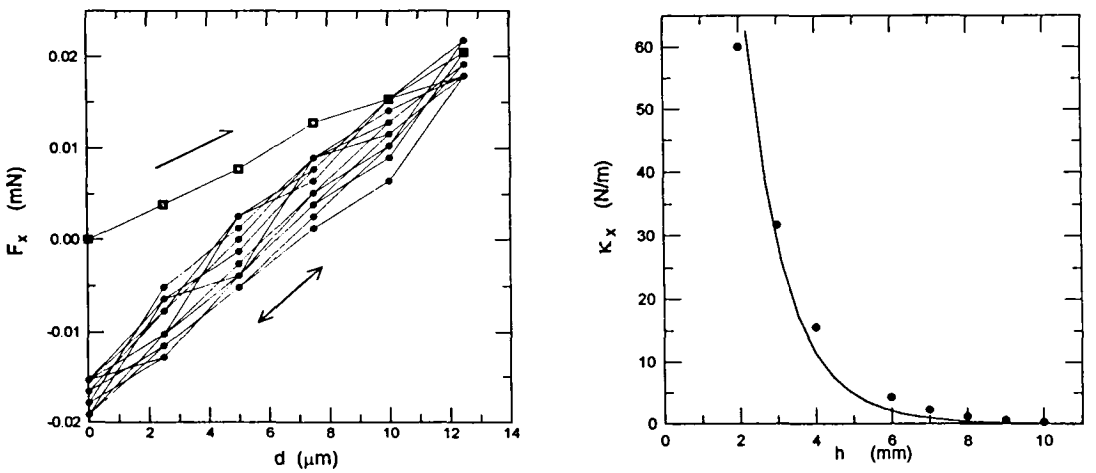

Figure 7: Horizontal restoring force versus displacement(left) together with experimental and theoretical horizontal stiffness, κ_x, as function of levitation height.(right)

Figure 7(left) shows the observed behavior of the lateral force during a virgin horizontal displacement followed by small-amplitude oscillations. The positive slope of the unique virgin branch quantifies the lateral stability of the system. On return to $d = 0$ the F_x becomes negative. The subsequent oscillations produce a linear force–displacement relation with a steeper slope that represents the lateral stiffness κ_x. The experiment was done using the same HTSC-PM system as in the previous sections, also now providing z.f.c. to 77K. The distance was here $h = 7$mm, and the

initial position, $d = 0$, corresponds to the symmetrical configuration of fig.1. The measurements were repeated at different distances to find the h-dependence of the stiffness, fig.7(right).

We calculate the lateral force from

$$F_x = \int_V M \frac{\partial B_x}{\partial z} dV = l\, t_b \int_{-b}^{b} dx\, M \frac{\partial B_z}{\partial x} . \tag{14}$$

where, as before, the thin sample approximation was used. Note immediately that for the initial symmetric position F_x vanishes since M is symmetric in x and $\partial B_z/\partial x \equiv g(x)$ is antisymmetric.

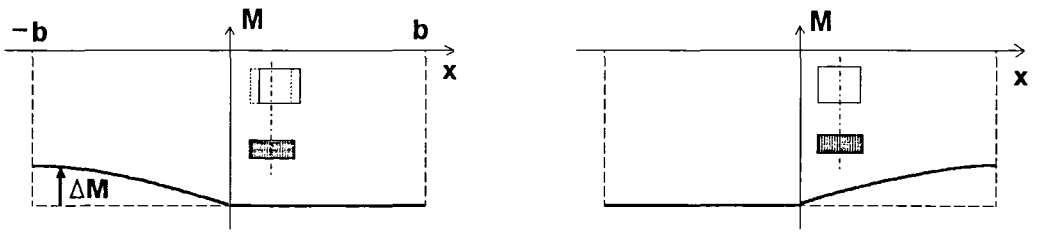

Figure 8: Profile of the magnetization after a lateral displacement of the magnet (left), and after completing one displacement cycle(right). In the model $\Delta M = f_s|\Delta B_z|/\mu_0$ is the deviation from uniform magnetization, $-M_{sat}$.

When the magnet is displaced a small distance d, the lateral shift in the field profile implies that B_z increases for $x > 0$ and decreases for $x < 0$. To 1. order the field change is

$$\Delta B_z = B_z(x-d) - B_z(x) = -g(x)\, d .$$

This will cause an asymmetry in $M(x)$ which we can evaluate as follows. Consider two grains located symmetrically on each side of $x = 0$. Initially, they both experience the same applied field, which we assume induces a negative magnetization corresponding to saturation. For the present range, $h \leq 10$mm, this is an assumption consistent with the analysis in section 3. After the lateral displacement the grain at $x < 0$, due to a field reduction, aquires an additional magnetization, $|\Delta B_z|/\mu_0$, whereas the grain at $x > 0$ remains in saturation since the field there has increased. The resulting M versus x is shown in fig.8(left). For $x < 0$ one has

$$M = -M_{sat} + \frac{f_s}{\mu_0}\, g(x)\, d .$$

One also has to take into account that the gradient $\partial B_z/\partial x$ has been shifted by d. To 1. order it is now $g(x-d) = g(x) - g'(x)\, d$, giving

$$F_x(d) = l\, t_b \left(\frac{f_s}{\mu_0} \int_{-b}^{0} [g(x)]^2\, dx - 2M_{sat}\, |g(b)| \right) d . \tag{15}$$

This describes the virgin force behavior, and represents a stabilization since the magnitude of the first term is much larger than the second.

To find the stiffness one needs to consider the effect of reversing the magnet motion. With the PM back to $d = 0$ the grain at $x < 0$ will have experienced one complete minor loop and has restored its state of saturation. On the other hand, a grain at $x > 0$ will experience a field reduction, and add a positive part to the magnetization. The new profile of M is shown in fig.8(right). Here the field gradient is once again the fully antisymmetric $g(x)$, and one gets

$$F_x(d=0) = -l\, t_b \left(\frac{f_s}{\mu_0} \int_{0}^{b} [g(x)]^2\, dx \right) d , \tag{16}$$

which describes the minimum force seen in fig.7(left)

By repeating this displacement cycle the magnetization will alternate between the profiles of fig.8, and F_x will oscillated linearly between the two extremum values given by eq.(15) and (16). The stiffness is therefore equal to

$$\kappa_x = \frac{F_x(d) - F_x(d=0)}{d} = 2\,l\,t_b\,\left(\frac{f_s}{\mu_0}\int_0^b [g(x)]^2\,dx - M_{sat}\,|g(b)|\right). \qquad (17)$$

The full line in fig.7(right) represents this expression using $f_s = 0.8$ and $M_{sat} = 1900$A/m found in section 3. The weak field dependence of the saturation magnetization was neglected since the main contribution to κ_x lies in the integral term. Again, we find a quite acceptable quantitative agreement between our data and the model calculation, where no parameters were adjusted. Theoretically, κ_x is about twice the slope of the initial stabilizing force. Within the experimental uncertainty also this prediction is consistent with the observed behavior.

Experimentally it has been found that when the amplitude of vibrations increases the PM-HTSC interaction becomes more and more dissipative.[9] This also follows from Bean's model where the energy loss per cycle for a long cylinder in a parallel field equals[14]

$$W = \frac{2V}{3\mu_0}\left[\frac{2(\Delta B)^3}{B^*} - \frac{(\Delta B)^4}{(B^*)^2}\right] \text{ for } \Delta B \le B^* \text{ and } W = \frac{2V}{3\mu_0}\left[2B^*\Delta B - (B^*)^2\right] \text{ for } \Delta B \ge B^* \qquad (18)$$

Here ΔB is the amplitude of the external flux density, which in the mechanical case is determined by the displacement amplitude of the PM. In order to design an optimal vibrational damper for a given application one will probably need to tune the dissipation properties of the system. Note then that one way to vary the ac-loss at a given vibrational amplitude is to modify the full penetration field, B^*. This parameter is proportional to j_c, which again depends on temperature.

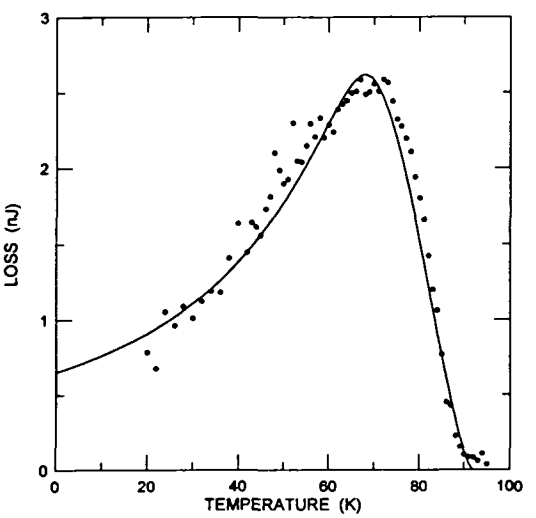

Figure 9: ac-loss per cycle in lateral vibrations of 50μm amplitude. The line represents the theoretical temperature dependence of the dissipation.

Figure 9 shows the result of a measurement series of the ac-loss in lateral vibrations maintained at a constant amplitude of 50μm over a range of temperatures. The dissipation was determined from the area of the force-displacement loops. As found also in numerous susceptibility measurements, the loss varies strongly with the temperature, having here a peak near $T^* = 70$K. At this maximum the magnitude of $j_c(T^*)$ is such that the 50μm displacement amplitude satisfies the condition $\Delta B = B^*$, where due to the distribution of grain sizes B^* must be understood in an

average sense. The expressions of eq.(18), modified by $V \rightarrow f_s V$ to account for the magnetic porosity of the HTSC, were fitted to our loss data. A temperature dependence of j_c of the form $j_c(T) \propto (1 - T/T_c)^p$ was assumed. Best fit was obtained for $p = 3/2$, and the result is seen in the graph as a full line. Again a very good quantitative agreement is obtained.

A detailed description of the loss experiment together with a more comprehensive theoretical analysis will be published soon.[15]

5. CONCLUDING REMARKS

Several key parameters characterizing the mechanics of magnetic levitation with HTSCs have been investigated experimentally and theoretically. We have shown that (1)the repulsive vertical force and its associated stiffness, (2) the lateral stabilizing force and the stiffness governing horizontal vibrations and (3) the temperature dependence of the mechanical ac-loss can be explained at a quantitative level and with a minimum of adjustable parameters. For the first time, analytical expressions for all these quantities have been derived consistently for a model system. By doing so it is brought out in detail how different parameters such as geometry and the magnetic response of the superconductor affect the behaviors.

In this work we chose to study a sintered HTSC instead of a melt-processed bulk sample. The reason is that melt-processed HTSCs tend to consist of grains many orders of magnitude larger than in sintered samples. Although large grains give rise to large levitation forces, it will also produce a local magnetization that varies over distances of the same scale as the size of the levitating magnet. To account quantitatively for the forces in such cases one probably needs to consider the detailed structure of weak links, or the large-scale flow pattern of the shielding currents in each individual HTSC sample. This problem was avoided here by averaging over many small grains.

The authors wish to thank prof. Y. Galperin for stimulating discussions. The financial support by The Research Council of Norway (Norges Forskningsråd) is gratefully acknowledged.

References

1. B.R. Weinberger, L. Lynds and J.R. Hull, Supercond. Sci. Technol. **3**, 381 (1990).
2. F.C. Moon, C.Golkowski and D. Kupperman, Appl. Supercond. **1**, 1175 (1993).
3. K.B. Ma, C.K. McMichael, M.A. Lamb and W.K. Chu, IEEE Trans. Appl. Supercond. **3**, 388 (1993).
4. I.-G. Chen, J. Liu, R. Weinstein and K. Lau, J. Appl. Phys. **72**, 1013 (1992).
5. see e.g., F.C. Moon, "Magneto-Solid Mechanics", New York, John Wiley & Sons, 1984.
6. F. Hellman, E.M. Gyorgy, D.W. Johnson Jr., H.M. O'Brian and R.C. Sherwood, J. Appl. Phys. **63** 447, (1988).
7. L.C. Davis, J. Appl. Phys. **67** 2631 (1990).
8. T. Torng and Q.Y. Chen, J. Appl. Phys. **73** 1198 (1993).
9. T.H. Johansen, H. Bratsberg, Z.J. Yang, S.J. Guo and B. Loberg, J. Appl. Phys. **70**, 7496 (1991).
10. A.A. Polyanskii, V.K. Vlasko-Vlasov, M.V. Indenbom and V.I. Nikitenko, Sov. Tech. Phys. Lett. **15**, 872 (1989).
11. C.P. Bean, Phys. Rev. Lett. **8**, 250 (1962).
12. Y.B. Kim, C.F. Hempstead and A.R. Strnad, Phys. Rev. **129**, 528 (1963).
13. T.H. Johansen, H. Mestl and H. Bratsberg, J. Appl. Phys. **75**, (1994).
14. R. B. Goldfarb, M. Lelental, C. A. Thompson in "Magnetic Susceptibility of Superconductors and Other Spin Systems" edited by R. A. Hein, T. L. Francavilla, D. H. Libenberg, New York, Plenum Press, 1991.
15. P.O. Hetland, H. Bratsberg and T.H. Johansen(to be published).